Effect of WC morphology on dry sliding wear behavior of cold-sprayed Ni-WC composite coatings

Sima A. Alidokht, Stephen Yue, Richard R. Chromik

PII: S0257-8972(18)31189-7
DOI: https://doi.org/10.1016/j.surfcoat.2018.10.082
Reference: SCT 23945

To appear in: *Surface & Coatings Technology*

Received date: 24 July 2018
Revised date: 26 October 2018
Accepted date: 27 October 2018

Please cite this article as: Sima A. Alidokht, Stephen Yue, Richard R. Chromik , Effect of WC morphology on dry sliding wear behavior of cold-sprayed Ni-WC composite coatings. Sct (2018), https://doi.org/10.1016/j.surfcoat.2018.10.082

Effect of WC morphology on dry sliding wear behavior of cold-sprayed Ni-WC composite coatings

Sima A. Alidokht, Stephen Yue, Richard R. Chromik*

Department of Mining and Materials Engineering, McGill University, M.H.Wong Building, 3610 University Street, Montreal, QC H3A 0C5, Canada

* corresponding author

Abstract

Cold spray is a relatively new method used to deposit WC reinforced composite coatings, where its low temperature is advantageous for avoiding oxidation and carbide decomposition. Previous studies demonstrated that using powders made from agglomerated WC resulted in higher WC retention in a sprayed coating when compared to that of cast WC. However, the influence of the morphology of the starting powders on the coating's microstructure, properties, and wear performance is not well understood. Here, we report cold spray deposition of Ni with two types of WC particles, i.e. cast and agglomerated. In both cases, ~30vol.% WC was retained in coatings, allowing for a side-by-side comparison. Coatings with cast WC featured a multi-modal distribution of WC particles ranging from 0.2 to 20 μm with a mean free path (MFP) between particles of 8.5 ± 0.7 μm. In comparison, coatings with agglomerated WC had WC size range of 0.3 to 1.3 μm and an MFP of 31 ± 4 μm. The sliding wear behavior of coatings was studied with a sliding speed of 3 mm/s under normal loads of 5 and 12 N. Coatings with cast WC were found to be more wear resistant than coatings with agglomerated WC. The multi-modal size distribution of cast WC with significantly lower MFP minimized adhesive wear and helped to develop a higher coverage of protective mechanically mixed layers (MMLs) that typically formed near WC particles. For coatings with cast WC, subsurface microstructure and chemical analysis suggested higher oxidation for MMLs with shallower depths of deformation in the metal matrix beneath the MMLs compared to coatings with agglomerated powder. The main factors for improved wear resistance of cast WC coatings compared to agglomerated WC coatings were the stability of the MMLs, and the wider size distribution with lower MFP, which offered better load supporting properties.

Keywords: Cold spray, Metal matrix composite, Friction, Mechanically mixed layer (MML), WC morphology, Subsurface microstructure

1. Introduction

Due to their exceptional wear resistance, metal matrix composites (MMCs) reinforced with WC have long been used in demanding engineering applications [1-4]. There are various methods to prepare MMCs of WC with metal matrices based on Co or Ni, including liquid phase sintering (LPS), hot isostatic pressing (HIP) and microwave sintering (MW). These wear resistant MMCs may also be prepared as coatings by various thermal spray methods, including HVOF, plasma spray, and cold spray. For all these processes, the feedstock powders play a role in optimizing the process and the properties of the MMCs [3, 5]. Several types of WC powder are used for the surface coating process, among which cast WC and agglomerated WC-Co or Ni powders are most often the materials of choice [1-4]. For the cast WC powder, induction plasma technology is often applied to transform crushed powders into dense spherical powders. During the spheroidization process, the feed particles are heated to melting point followed by cooling under controlled conditions [6]. The powder is a mix of eutectic WC and W_2C phases [6].

The low temperature of cold spray is advantageous through avoiding oxidation and carbide decomposition, which commonly occurs in thermal spray and laser cladding processes [7, 8]. Previous studies found that the recovery of WC particles to coatings during cold spraying are influenced by their morphology [9-13]. The dense structure of cast WC and their limited deformability causes fracture of WC particles during deposition and their loss. Whereas the porous structure of agglomerated WC particles along with Co/Ni binder between WC agglomerates provide ductility. This allows for deformation, densification, and elongation of agglomerated particles through slipping and rotation of WC particles along the Ni binder, leading to a significantly higher WC retention within the matrix. Previous studies reported high losses of cast WC particles with only 11-29% of WC retained into coatings [9, 12]. A significant improvement

in WC retention in coatings was obtained using WC agglomerated and sintered with Ni. The WC content in coatings was reported to be close to that of the initial feedstock [9, 11, 12]. It is important to note that, although there is a desire for higher recovery of ceramic particles into cold sprayed coatings, recent studies have shown higher retention of the ceramic particles may not necessarily lead to better tribological performance. The wear properties of WC composite coatings are influenced by WC particle fraction, morphology, distribution, metallic matrix microstructure, as well as WC/Ni interfacial bonding [14, 15]. Therefore, for future tribological applications of cold sprayed MMCs, both cold spray process optimization and characterization of the tribological performance is required.

During the sliding wear of metallic materials and MMCs against a counterpart, plastic deformation, material mixing, and the generation of wear debris take place. These mechanical processes are often accompanied by chemical reactions with the environment, most commonly oxidation. After some time, the imposed load, shearing stresses, mechanical mixing, and chemical reactions result in a surface oxide layer that is often referred to as a mechanically mixed layer (MML) [16-19]. The formation and stability of MMLs are closely associated with the wear performance of MMCs in sliding systems. Hard, stable, and continuous MMLs often reduce friction and wear [16-19]. Pure metals and alloys also form MMLs, but the hard phase present in MMCs is found to play a role in the oxidative wear mechanisms [20, 21]. The size and the interfacial bonding strength of the hard reinforcement particles to the matrix influence the critical oxide thickness, which determines the extent of reinforcement particles in providing protection against oxidational wear of the matrix [21, 22].

For an unreinforced material subjected to sliding wear, oxides grows progressively to a critical thickness where it becomes unstable and is subsequently removed from the surface. Fresh

metal contact is then established, leading to rapid wear. However, in the presence of hard particles, larger particles can offer load support, which will delay removal of the oxide layer, making it stable to a greater thickness. Smaller particles can be incorporated into the MML and enhance the properties, again leading to greater stability. When the MML is eventually broken down, the reinforcing particles underneath the MML become exposed and reduce metal contacts to the counterbody. At this stage, the load supporting nature of the particles as well as their cohesion strength with the metallic matrix determines their effectiveness on protecting the metallic matrix from wear [20, 21]. The critical oxide thickness can be in the range of 1-5 μm for metallic materials. Compressive stress within the oxide is caused by the expansion of the lattice, to accommodate the oxide growth. Beyond critical oxide thickness, the stress would be sufficient for adhesion loss and formation of wear debris [21, 22]. The previous discussion is for a "total oxide mechanism" for metals, where an oxide grows progressively to its critical thickness and then it is removed. However, it has also been reported that many of these concepts can be applied for the case of an oxide layer developed by the debris compaction [20].

In previous work of Alidokht *et al*. [12], room temperature sliding wear of a cold-sprayed Ni-10.5 vol% WC coating using cast WC was analyzed. A significantly lower wear rate compared to a cold-sprayed pure Ni coating was reported, due to the formation of a stable oxide film or mechanically mixed layer (MML) on worn surfaces. WC particles promoted the formation of an MML composed of Ni and W oxides and WC fragments. As reported in a previous study [13], using agglomerated WC, deposition and retention of WC can be significantly improved. Although there is a desire for higher recovery of ceramic particles into cold sprayed coatings in recent studies, it is not clear that higher retention of the ceramic particles leads to better tribological performance. Moreover, there is no systematic study where the two types of WC particles and their role in the friction and wear of Ni-based composite coatings have been compared.

In the present study, two Ni-WC coatings with a similar fill ratio of the cast and agglomerated WC were cold-sprayed. For the two composite coatings, dry sliding wear tests were conducted and the effect of WC particles morphology on the friction and wear was studied.

2. Experimental

Feedstock powders for cold spray were commercially pure water atomized Ni (4SP-10, Novamet, Kentucky, USA), plasma spheroidized cast WC (TEKMAT™ WC-45, Tekna, Canada), and agglomerated and sintered WCNi (AMPERIT® 547, H.C. Starck, Germany). A co-feeding system with two powder hoppers was used to spray composite coatings with various contents of WC, where the feed rate of Ni, WC or WCNi powder was varied. For each coating system, i.e. cast WC and agglomerated WCNi, four 3×1-inch steel substrates were coated. The structure and properties of these coatings are reported on in a previous study [13]. Here two composite coatings (one using cast WC and one using agglomerated WCNi) of roughly 30 vol.% WC was selected for side-by-side comparison of their tribological properties.

Coatings were deposited onto steel plates using a commercially available cold spray system (PCS-800, Plasma Giken, Japan). The cold spray unit utilized a de Laval nozzle made of WC-Co. Nitrogen was used as the process gas. The gas pressure was 4 MPa, the gas preheat temperature was 700°C, the stand-off distance between the substrate and nozzle exit was set at 40 mm and the gun traverse speed was 30 mm/s.

Cold-sprayed coatings were cross-sectioned perpendicular to the gun traverse direction, mechanically ground, and polished using 9, 3 and 1 μm diamond pastes followed by 0.05 μm colloidal silica. The morphology and microstructure of the initial powders and deposited coatings were observed by scanning electron microscopy (SEM) (FEI Quanta 600, Thermo Fisher Scientific,

USA). The WC and porosity concentrations within the coatings were measured from at least three specimens that randomly were cross-sectioned from four coated samples. Ten random images of polished cross-sections were collected for each specimen in an SEM, then analyzed by pixel count using an open source software ImageJ. To estimate mean free path (MFP) between WC particles, SEM images of polished cross-sections of coatings was analyzed using ImageJ image analyzing software. A random line was drawn on the images and the number of times that the line intersects the WC particles was noted. The line distance was measured using the measure distance function, in which pixels counts are converted into micrometers according to the scale bar of the corresponding image. Then, the number of particles intersects per unit length of the line, N_l, together with the volume fraction of WC particles, v_p, was used to estimate the MFP of the WC particles (λ) using following equation [23-25],

$$\lambda = \frac{1-v_p}{N_l} \qquad (1)$$

At least 50 measurements were made to obtain an average value for MFP of the WC particles for each coating system.

The two coatings selected for the present study contained 28 vol.% cast WC and 30 vol.% WC in the form of agglomerated WCNi, with assigned designations of Ni-castWC and Ni-aggWC, respectively. To characterize the mechanical properties of cold sprayed coatings, nano-hardness and micro-hardness testing were used. Nano-indentation using a Berkovich diamond tip with a triboindenter system (TI 950, Hysitron, USA) was performed on the polished cross-section of coatings to measure mechanical properties of Ni matrices. The peak load, loading and unloading rate, and hold time at peak load are fixed as 5 mN, 200 μN/s, and 2 s, respectively. To calculate hardness and elastic modulus, the indentation unloading-displacement data were analyzed using the Oliver and Pharr method [26]. Vickers micro-indentation (Clark CM-100AT, Clarke

Instruments Ltd, UK) was performed on top polished surfaces. To obtain an average hardness value of the composite, a large load of 1 kgf with a dwell time of 15 s on a micro-hardness tester was used.

Sliding wear tests on the coatings were performed in dry air (below 3% relative humidity) using a custom-built ball on flat reciprocating tribometer. Prior to the wear test, the coatings were polished to a final step by 0.05 μm colloidal silica. Spheres of WC-Co (McMaster Carr, USA) with a diameter of 6.25 mm were used as counterfaces. All wear tests were also conducted with normal loads of 5 and 12 N, sliding speed of 3 mm/sec, and track length of 5 mm. Tests were run to 10, 50, 100, 500, and 1000 cycles. Friction forces were measured with a sampling rate of 800 Hz using a piezoelectric sensor mounted underneath the sample stage. Along each cycle, the coefficient of friction (CoF) was averaged across a central portion of the track and then graphed versus the number of cycles. Worn samples were examined using a non-contact optical profilometer (NewView, Zygo instruments, USA) to obtain profiles of the wear tracks. The volume of material removed, v, was measured by multiplying the cross-sectional area of material removed, measured by profilometry, by the track length. The cross-sectional area was determined by integrating height profiles across the wear track above and below the original surface, where a total number of 50 - 60 surface profile measurements per wear track were used. This, along with the total sliding distance x and applied load W, was then used to calculate the wear rate, $\acute{k}$ (mm^3 /Nm) using the equation (1) [27],

$$\acute{k} = \frac{v}{Wx} \qquad (2)$$

The above-mentioned procedure and Eq. 2 have been used to estimate the wear rate of HVOF and cold-sprayed coatings in previous studies [23, 28]. In order to study wear mechanisms, worn surfaces and cross sections of wear tracks were examined using an SEM (FEI Quanta 600,

Thermo Fisher Scientific, USA) equipped with energy dispersive X-ray spectroscopy (EDS). To measure mechanical properties of third-bodies, Nano-indentation was also performed on wear tracks and on the cross section of worn surfaces at a peak load of 1 mN. All other indentation parameters and setup was explained above. Subsurface morphologies of the wear tracks were examined with a Cryo-STEM (FEI Tecnai G2 F20, Thermo Fisher Scientific, USA). TEM specimens were made with a focus ion beam (FIB) lift-out performed using a DualBeam SEM (FEI Helios Nanolab 660, Thermo Fisher Scientific, USA).

3. Results

3.1. Coatings

For the Ni-castWC and Ni-aggWC coatings, Table I summarizes the WC fraction, porosity and micro-hardness of coatings, nano-hardness of Ni matrices, and MFP between WC particles. Figure 1 shows the micrographs of the cross-sectioned composite coatings. Using WCNi composite powder, the retention of WC in the coating was significantly improved and WC content was close to that of the initial feedstock. Particle retention mechanisms and WC fill ratios for various mixtures were discussed in detail in an earlier work [13]. No significant fracture of WC particles was observed in Ni-aggWC coating. However, most of the cast WC particles were cracked/fragmented, leading to WC fragments consisting of particles size ranges from 0.2 to 20 μm. The addition of WC particles enhanced the hardness of coatings. Comparing the micro-hardness values of the two composite coatings, cast WC particles were more effective in hardening the coatings. This is due to significantly lower MFPs between WC particles in Ni-castWC compared to that of the Ni-aggWC coatings (see Table I). The higher nano-hardness of Ni matrix in Ni-castWC coatings is due to ultra-fine (<1 μm) WC fragments caused by severe fragmentation upon impact.

Table I Characteristics of cold-sprayed Ni-castWC and Ni-aggWC coatings [13].

Sample designation (this paper)	Sample designation in [13]	WC in feedstock (vol%)	WC in coatings (vol%)	Porosity (%)	Hardness (HV_{1kg})	Ni matrices hardness (GPa)	MFP (µm)
Ni	Ni	-	-	3.8 ± 0.5	345 ± 17	4.8 ± 0.9	-
Ni-castWC	Ni-30WC/Ni	80	28 ± 4	0.3 ± 0.1	431 ± 26	5.1±0.8	8.5 ± 0.7
Ni-aggWC	Ni-28WC(30)	36	30 ± 5	0.5 ± 0.2	390 ± 27	4.5±0.6	31 ± 4

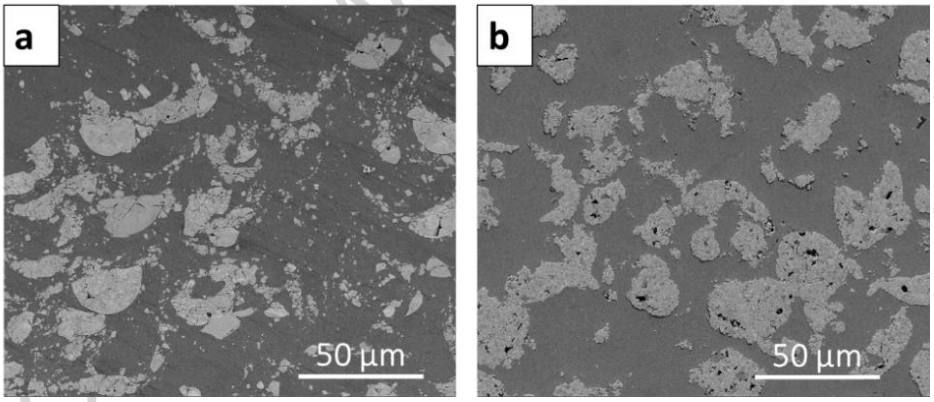

Fig. 1 Secondary electron (SE) images of unworn microstructures of (a) Ni-castWC and (b)Ni-aggWC viewed in the cross-section.

3.2. Friction and Wear

For sliding wear tests at two loads of 5 and 12 N, both coatings, Ni-castWC and Ni-aggWC, showed similar CoF behavior (Fig. 2), developing higher CoF values during the run-in period,

before reaching steady-state values. The Ni-castWC coating sliding under 5 N load showed a run-in period until 190 cycles followed by steady state friction coefficient value of 0.69. The CoF curve at 12 N reached steady state at a longer distance (250 - 300 cycles) and its steady-state value was 0.74. Run-in periods for Ni-aggWC coatings tested under 5 N lasted up to longer cycles (250 cycles), compared for those observed for Ni-castWC coatings. Similar to Ni-castWC coating, a higher steady-state value was recorded at 12 N (0.74) compared to that at 5 N (0.63). This is attributed to an increase in the contact area and hence frictional contact at higher load. Under 5 N applied load, Ni-castWC coatings exhibited a higher CoF compared to that of Ni-aggWC coatings; however, for 12 N, the steady-state values for both coatings were around the same value of 0.74. The friction behavior of Ni-aggWC was considerably less stable than that of Ni-castWC. A higher fluctuation in CoF was observed at the lower load of 5 N for Ni-aggWC coating, where the CoF fluctuated between 0.60 and 0.68, with many temporary drops and shifts to plateau values. Large fluctuations in CoF for Ni-aggWC coating at 5 N are attributed to the formation of wear debris and its recirculation throughout the contact interfaces. Sliding tests were repeated at least 5 times for each condition. For both coatings, friction trends were repeatable. For Ni-castWC coatings, the steady state was much more stable in each instance when compared to friction behavior of Ni-aggWC coatings. Friction curves shown in Fig. 2 were close to the mean value per cycle for each instance. Steady-state CoF values, averaged from all tests, were 0.70 ± 0.07 and 0.73 ± 0.04 for Ni-castWC, and 0.63 ± 0.03 and 0.73 ± 0.02 for Ni-aggWC, at 5 and 12 N, respectively.

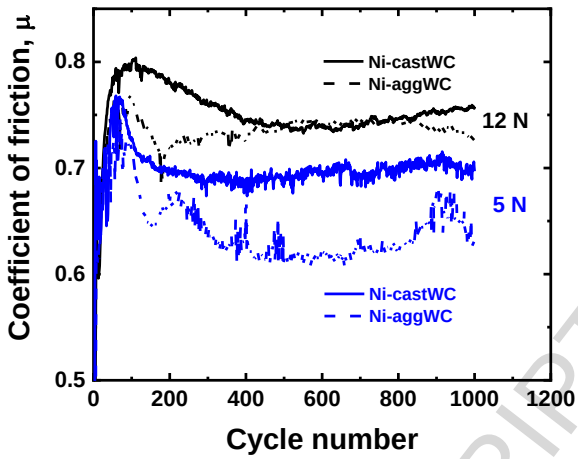

Fig. 2 Representative coefficient of friction versus sliding distance at 5 and 12 N of cold sprayed Ni-castWC and Ni-aggWC coatings.

Surface profiles of the wear tracks for the two coatings tested under two loads of 5 and 12 N are shown in Fig. 3. For Ni-castWC coating tested at 5 and 12 N, the worn surface exhibited an elevated MML, which has a greater height relative to its surrounding surface and unworn surfaces. Wear track topography (see Fig. 3c and d) of Ni-aggWC reveals a sharp contrast when compared to Ni-castWC coatings. The MML appeared as islands. Moreover, areas having a lower depth, around 4-6 μm, were continuous. For Ni-aggWC, at 5 N, elevated MML was observed, whereas, at 12 N, MML was at a lower height as compared to unworn surfaces yet elevated compared to regions inside wear track with mostly 4-6 μm depth.

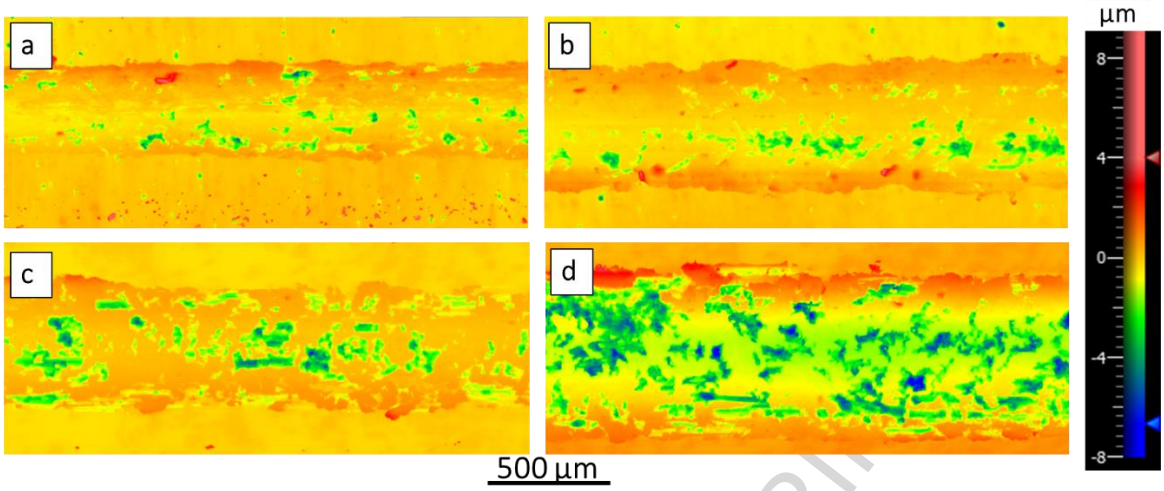

Fig. 3 Wear track topography of Ni-castWC at 5 N(a) and 12 N(b), and Ni-aggWC at 5 N(c) and 12 N(d).

The wear rates at the end of the 50 and 1000 cycles tests were calculated using equation (1) and presented in Fig. 4. The Ni-castWC coatings were found to be more wear resistance when compared to Ni-aggWC coatings. The wear rate measurement on Ni-castWC coatings was indicative of volume gain by these coatings after 1000 cycles. Whereas, for some tests, a very low material loss was recorded after 50 cycles, reflected as higher standard deviations in the wear rates (Fig. 4). However, for Ni-aggWC, mild wear rate values of 7 and 36×10^{-6} mm^3 /Nm for 5 and 12 N were measured after 1000 cycles, respectively. Increasing the load from 5 to 12 N, mean wear rates of Ni-aggWC increased by a factor of 5.

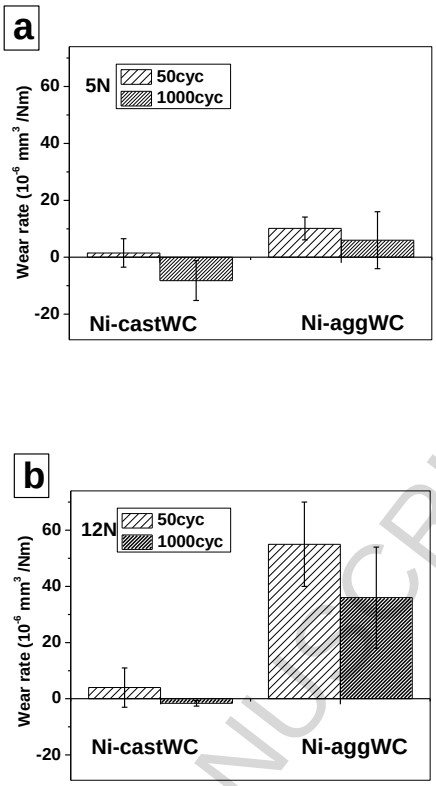

Fig. 4 Volumetric wear rate for Ni-castWC and Ni-aggWC tested at (a) 5 N and (b)12 N.

Wear rates of the WC-12Co counter-spheres after 1000 cycles sliding tests are given in Fig. 5. The Voigt and Reuss bounds were used to predict the upper and lower bounds of the elastic modulus of composite coatings and then used to calculate the corresponding upper and lower bounds of initial Hertzian contact pressure. The initial mean Hertzian contact stress [29] for composite coatings was estimated to be 821-827 MPa and 1082-1198 MPa, for 5 and 12 N, respectively. Both coatings caused wear of counterparts. Wear of counterparts during sliding contributed to a drop in the contact pressure. The apparent contact stresses after 1000 cycles sliding for Ni-castWC coatings were estimated to be 94 and 168 MPa, tested at 5 and 12 N, respectively. While WC–Co ball mating with Ni-aggWC coating underwent more severe wear, which may come from the higher amount of abrasive wear debris generated during the wear process. This led to the lower contact stresses after 1000 cycles, 62 and 139 MPa, under 5 and 12 N, respectively, when

compared to Ni-castWC coatings. For both coatings, the higher load led to higher wear on counter-spheres, increasing sliding contact areas. However, despite significant ball wear for both cases, overall the Ni-castWC sample remained more wear resistant than the Ni-aggWC sample.

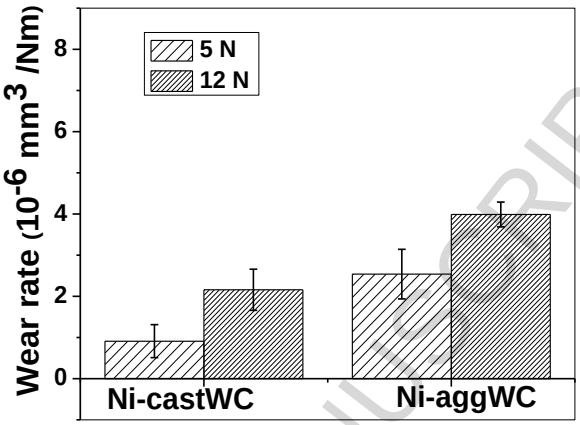

Fig. 5 Volumetric wear rate at 1000 cycles plotted for counter-spheres mating with Ni-castWC and Ni-aggWC coatings at 5 and 12 N.

3.3. Worn surfaces morphologies

Figures 6 shows worn surface morphologies of Ni-castWC during initial sliding cycles (i.e. 10 and 50). Tongue-shaped features, indicative of adhesion of Ni to the countersphere, were observed in areas where less WC was present at the surface. However, these features were less frequently observed here compared to a pure Ni coating tested in a previous study [12], which indicates some effectiveness of WC at reducing adhesive wear. Evidence was also found that Ni adhering to the countersphere was sometimes transferred back on the WC particles (Fig. 6a). Evidence of abrasive wear was also observed. Pulled out WC fragments and oxidized or work-hardened metallic debris can act as abrasive particles. Fine scratching marks in the direction of sliding were also observed and indicative of abrasive wear caused by hard particles (Fig. 6a). From

the size of scratching marks on the center and sides of the wear tracks, it appears that only small WC particles were dislodged from the surface and moved along sliding. As sliding continued, the wear debris was compacted between the sliding surfaces and developed areas of wear-protective oxide, MML (Fig. 6b and d). EDX analysis (not shown) showed oxidation of the surface, especially in the area of the MML and of the debris.

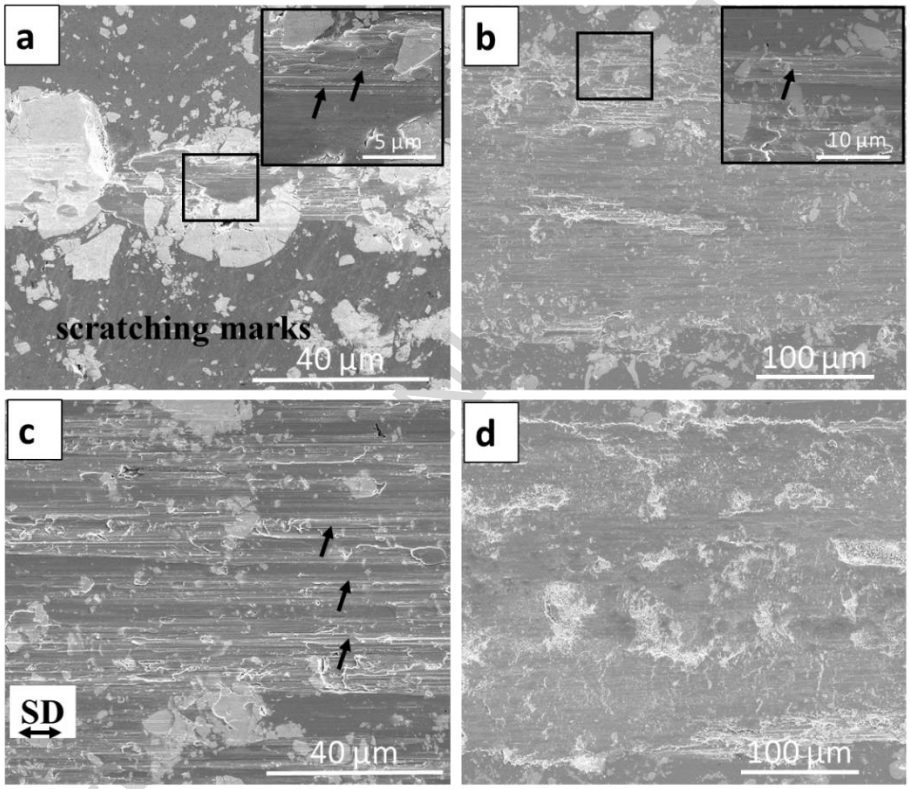

Fig. 6 Wear track topography of Ni-castWC after 10cycles (a) and (c), 50 cycles (b) and (d) at 5 and 12 N, respectively. Black arrows show scratching marks.

Worn surface morphologies of Ni-aggWC developed during initial sliding cycles (Fig. 7) were different from those for Ni-castWC coatings (Fig. 6). This indicated a different effect of the two WC particles types due to their different structures. Adhesive wear was much more intense in Ni-aggWC coatings, despite having a similar fill ratio of WC particles as Ni-castWC coatings (Fig. 7a and c). Formation of large metallic debris, as well as decohesion of WCNi particles and re-distribution of WC fragments over the wear track, occurred (see inset in Fig. 7a and d). Extensive

scoring of the surface in the sliding direction was observed on the Ni-aggWC coating worn surface (see Fig. 7a and c). As the tests progressed, the formation of MMLs became more evident (Fig. 7 b and d), but MML coverage was significantly lower than that of the Ni-castWC composite coating. In addition, at some regions on the wear track, the MML became damaged and partially escaped from the contact area (Fig. 7b). This exposed clean metal beneath for further oxidation and wear. Adhesive wear can be seen even at longer cycles of 50, as indicated by tongue-shaped features. A close comparison of the worn surfaces tested at two loads revealed that the extent of wear was significantly higher in Ni-aggWC tested at 12 N as compared to that at 5 N. EDX analysis (not shown) of the initial cycles worn surfaces were indicative of oxidation of the surface.

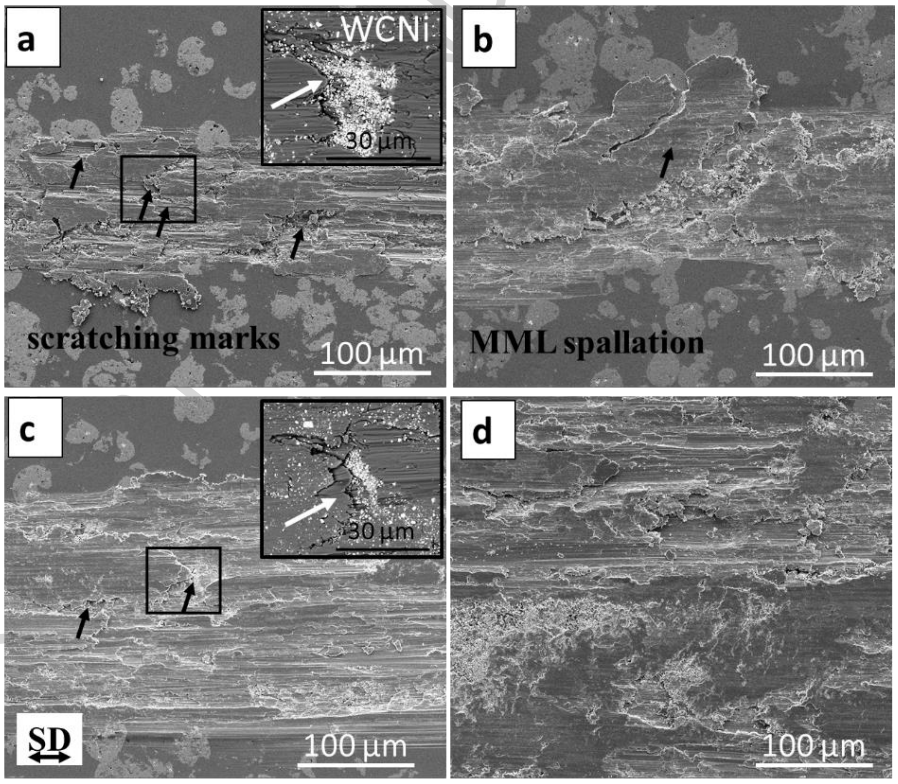

Fig. 7 Wear track topography of Ni-aggWC after 10cycles (a) and (c), 50 cycles (b) and (d) at 5 and 12 N, respectively. Black arrows show adhesive wear. White arrows indicate WC dislodgments.

Figures 8 shows worn surface morphologies of mating surfaces at the end of 1000 cycles sliding tests for Ni-castWC coatings tested under 5 and 12 N. Image analysis through pixel counting was used to measure the coverage ratio of MML on the worn surfaces, which has a greater height relative to its surrounding surface. Wear tracks were covered by MML with relatively high coverage of 85% and 89% at 5 and 12 N, respectively (Fig. 8a and d). MMLs were smooth (Fig. 8b and e) with very few scratch marks. However, some fatigue cracks were observed on MMLs (inset in Fig. 8c). BSE images with greater contrast between the Ni and WC showed the distribution of WC fragments on the worn surfaces (Fig. 8b and d). A previous study showed that the presence of WC fragments provided MML with resistance against plastic deformation and contributed to its stability [12]. No distinct change was observed by increasing the load from 5 to 12 N, except slightly higher MML coverage at 12 N.

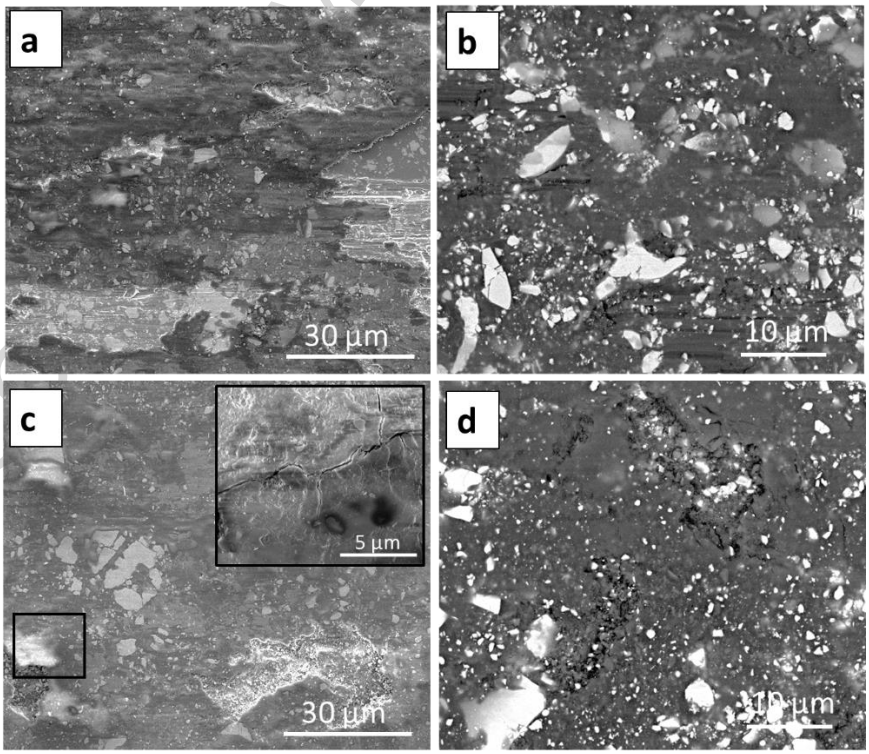

Fig. 8 Wear track topography of Ni-castWC after 1000cycles (a) at 5 N, (c) at 12 N, (b) and (d) higher magnification BSE images of (a) and (c), respectively.

Worn surface morphologies of Ni-aggWC coatings at the end of 1000 cycles sliding tests under 5 and 12 N are shown in Fig. 9, which showed different features compared to the Ni-castWC coatings (Fig. 8). Features that were observed on the surface of Ni-aggWC coatings indicated higher damage, as compared to those on Ni-castWC coatings. MML coverage on the surface was around 50% for the tested loads (Fig. 9a and b), which was significantly lower compared to Ni-castWC coatings. Higher magnification view of the MMLs revealed cracking of the oxide layer, leading to plate-like debris detachments (inset in Fig. 9a and b). BSE images of worn surfaces for Ni-aggWC coatings showed that WC particles distribution was modified during sliding, however, in this case, it was quite non-uniform (see Fig. 9b and d). The wear track of the Ni-aggWC coatings at 12 N displayed similar morphology to that at 5 N, except the amount of wear debris on the wear track which was significantly decreased (see Fig. 9a and c).

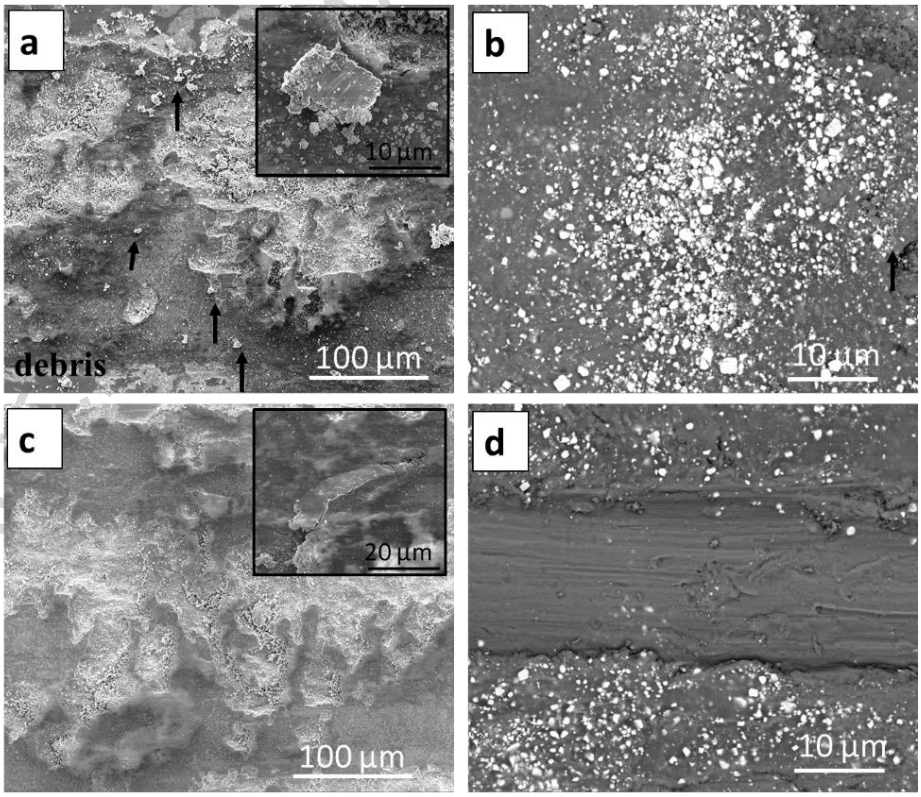

Fig. 9 Wear track topography of Ni-aggWC after 1000cycles (a) at 5 N, (c) at 12 N, (b) and (d) high magnification BSE images of (a) and (c), respectively. Black arrows show wear debris. Inset in (a) and (c) shows cracking and plate-like debris formation.

The scale of the wear debris was also correlated to tribological behavior. Figure 10 shows the morphology of the wear debris outside the wear tracks for Ni-castWC composite coatings. The Ni-castWC coating, with smaller wear debris, exhibited a lower wear rate than the Ni-aggWC coating, with larger wear debris (see Fig. 10a and b). Large plate-like debris can be observed (Fig. 10b indicated by arrow) was observed for Ni-aggWC coatings. Whereas, in the Ni-castWC worn surfaces, under both loads, compacted fine wear debris of 0.1 - 2 μm in size was observed.

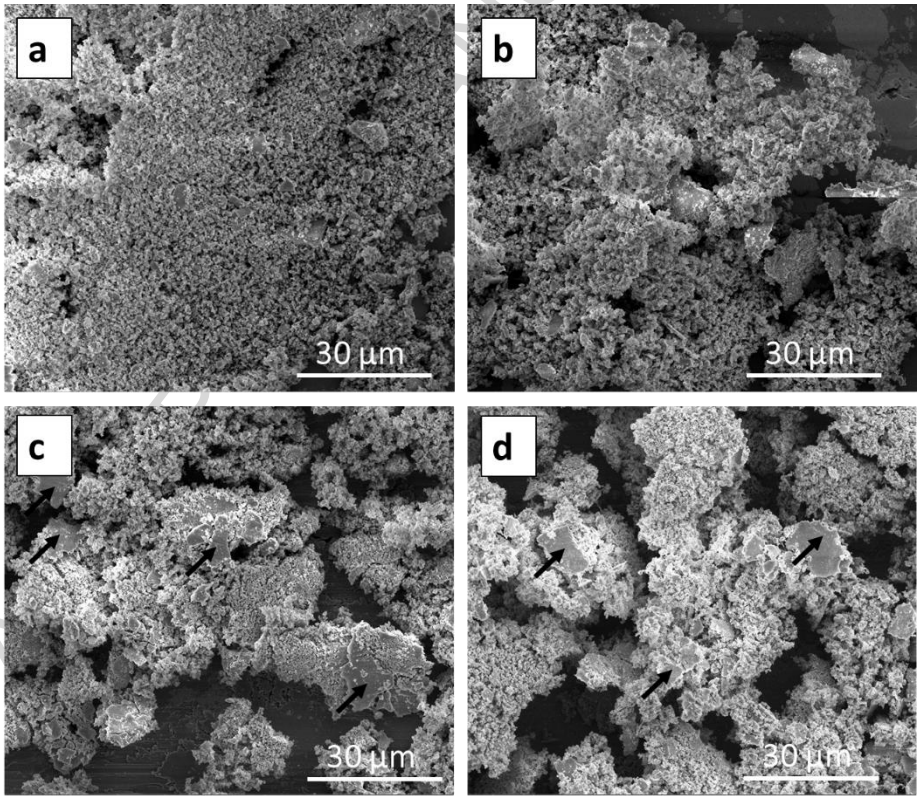

Fig. 10 Morphology of wear debris outside the wear track of (a) and (b) Ni-castWC, (c) and (d) Ni-aggWC tested under 5 and 12 N, respectively.

3.4. Raman analysis of worn surfaces

Raman spectra were collected on the MML of the two coatings to identify the chemical phase compositions. For Ni-castWC, Raman analysis indicated that the oxidation of Ni and W started from early cycles, with the NiO and WO_3 peak detected at ~550, and 800 and 930 cm^{-1}, [30] respectively (see Fig. 11a). Increasing sliding distance led to an increasing amount of NiO and WO_3 phases (see Fig. 11a). In addition, there was a new tribochemical phase of $CoWO_4$ and/or $NiWO_4$ (Co- or Ni- tungstate) at ~890 cm^{-1} [30], which started to form at 50 cycles (see Fig. 11a). $CoWO_4$ and $NiWO_4$ are very Raman active compounds, where a very thin layer of a few nanometers produces detectable peaks. No metal oxides were detected in the Raman spectra for the Ni-aggWC tested under the two loads of 5 and 12 N for initial cycles of 10 (see Fig. 11b). As the sliding progressed, WC agglomerates oxidized to WO_3 due to deformation induced by sliding. Using Raman analysis, the MML developed on the Ni-aggWC at 5 N was identified as containing NiO and WO_3. However, at a higher load of 12 N, the MML contains the mechanically mixed $CoWO_4$ and/or $NiWO_4$ tribochemical phase as well, as shown by the Raman spectra in Fig. 11.b. Representative EDX spectra that were obtained from MMLs of composite coatings are shown in Fig. 11c, where the Kα peak of oxygen and the Lα peak of Ni and Co are centered at 0.52, 0.85 and 0.77keV, respectively. Elemental composition analysis of the MML revealed increased oxygen in the wear scar. Semi-quantitative analysis of the EDX relative intensities showed a very low amount of Co, indicating that the $NiWO_4$ is the major phase in the MML. However, another possible instance could be a relatively thin layer of highly Raman active Ni- and/or Co- tungstate being present at the surface that is detected by Raman spectroscopy. Whereas, a quite large interaction volume is encountered by EDX beam and X-rays are emitted from much larger depth, where Ni is the major element. It is worth pointing out that Raman analysis of unworn WC-Co countersphere (not shown here) revealed no Raman active phase, except two peaks at 1350 and

1600 cm^{-1}, which corresponds to WC. Thus, the oxide layer predominately formed due to the tribo-chemical reaction during sliding.

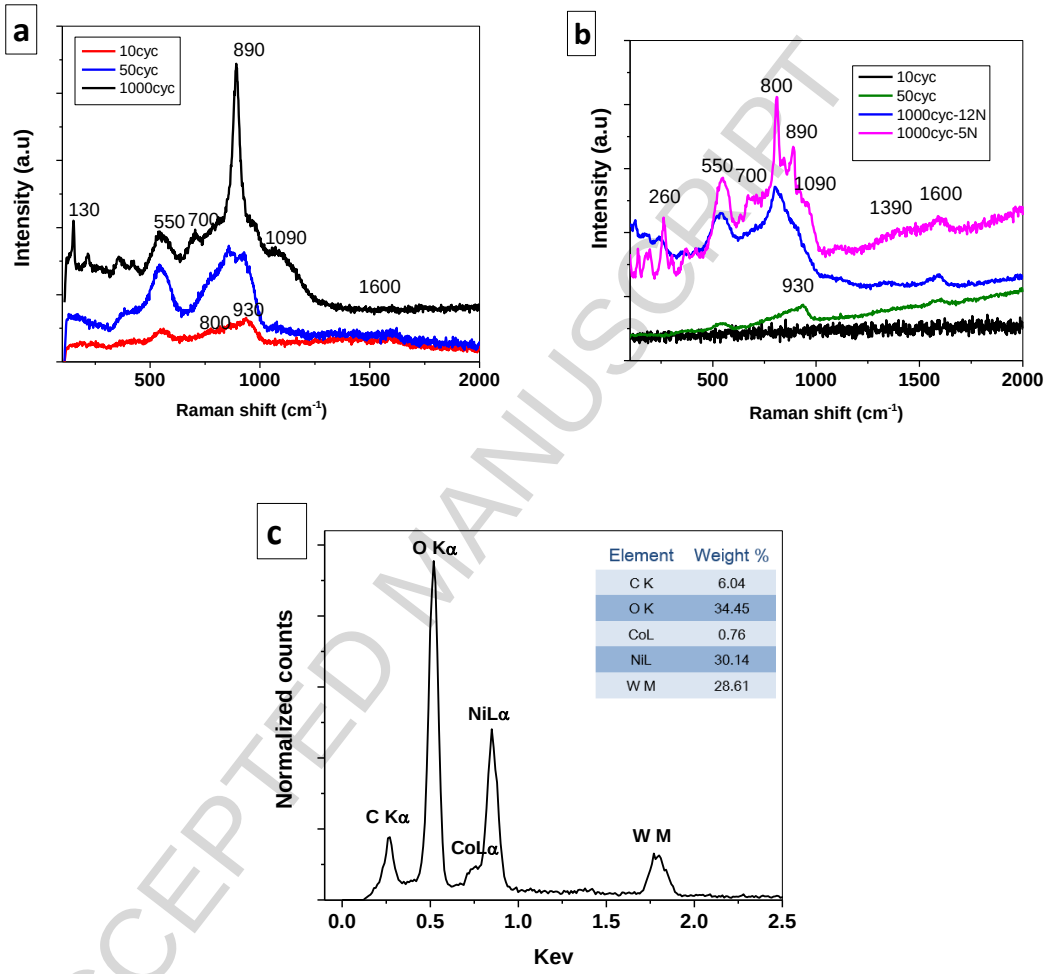

Fig. 11 Raman spectra of the MMLs obtained from (a) Ni-castWC and (b) Ni-aggWC coatings, (c) typical EDX spectra obtained from MML of composite coatings.

Figure 12 shows SEM images of the WC-Co counterfaces with a normal load of 12 N and corresponding Raman spectra acquired on the counterfaces after sliding for 1000 cycles on the Ni-castWC and Ni-aggWC coatings. Raman analysis showed that the ejected wear debris on the WC-Co counterface side is composed of NiO, WO_3, and $Co/NiWO_4$, which are the same tribochemical

phases present on the wear track surfaces, as shown in Fig. 11. A Raman spectrum on the plate-like debris found on the edge of counterface mating with Ni-aggWC in Fig. 12b showed that oxidation degree is less than the fine debris. SEM images showed that the counterface exhibited a wear flat and Raman spectroscopy analysis determined that there is no evidence of an oxide containing transfer film on the counterfaces.

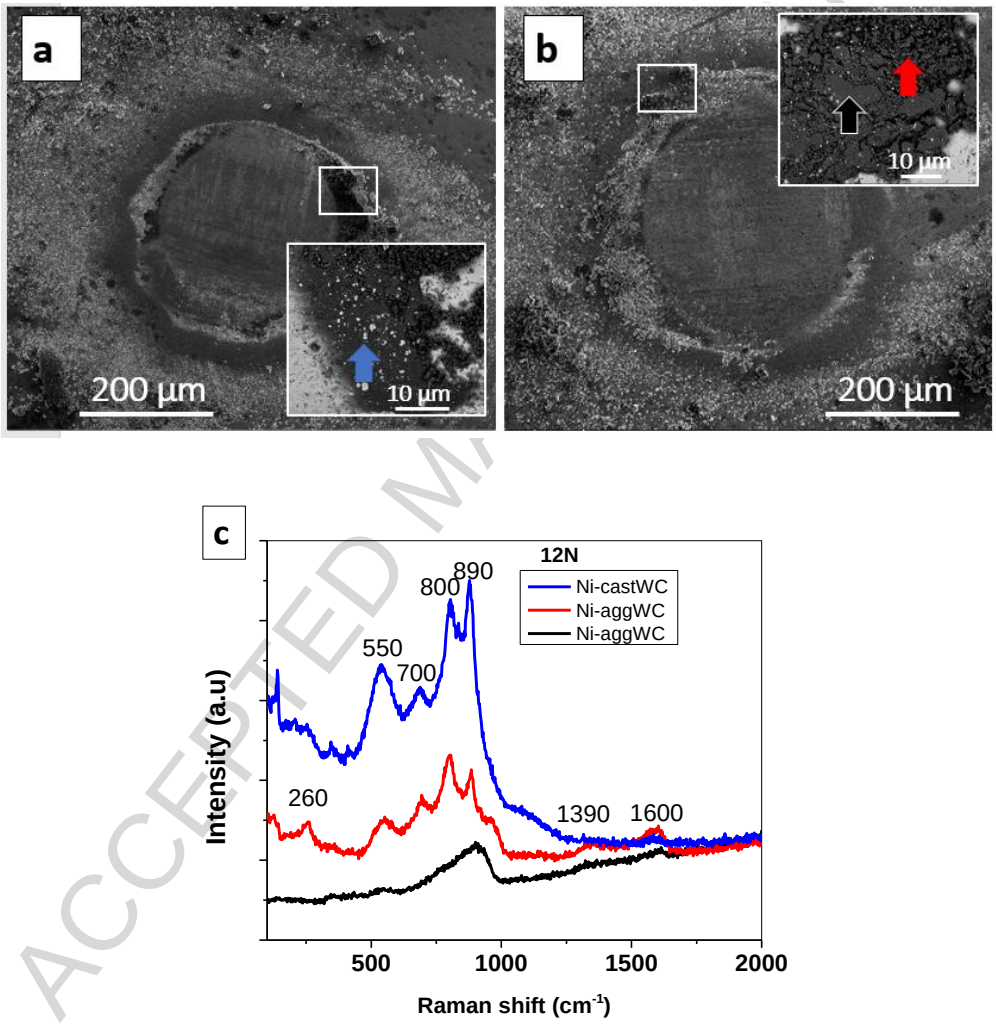

Fig. 12 SEM images of WC-Co counterfaces after 1000 cycles sliding on (a) Ni-castWC coating and (b) Ni-aggWC, under 12 N, (c) Raman spectra of wear debris on the WC-Co counterfaces. The arrows in the SEM images indicate the location for each Raman spectra.

3.5. Subsurface microstructure and hardness

In order to see additional details on the near-surface MML, TEM and selective area electron diffraction (SAED) was performed on a cross-sectional thin foil on the surface of the wear tracks. Subsurface microstructure observation of the Ni-castWC and Ni-aggWC wear tracks tested under 12 N was carried out through a FIB cut across MMLs, a typical feature developed for both coatings (see Fig. 13).

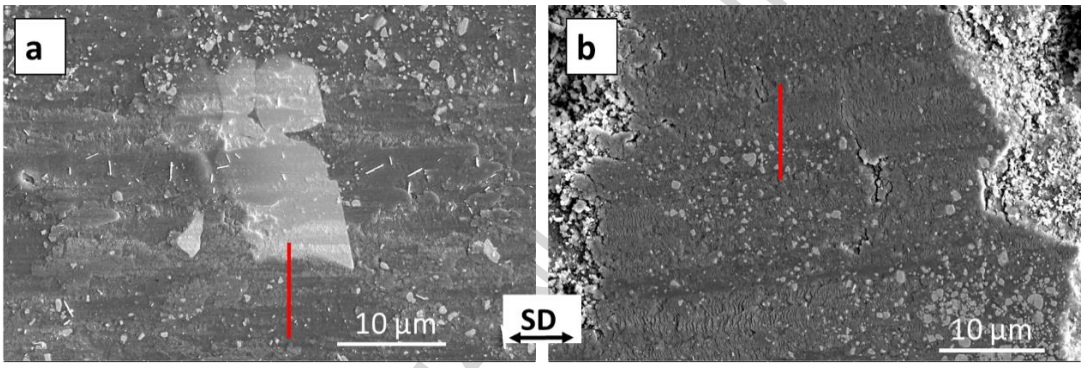

Fig. 13 Location of TEM foils obtained through FIB cutting on wear track of (a) Ni-castWC and (b) Ni-aggWC after 1000 cycles of wear under 12 N.

For Ni-castWC, TEM images revealed an MML with uneven thickness (Fig. 14a). The MML was thicker (~2.4 µm) where it is supported by a relatively big WC particle. Using a higher magnification image of the MML, fine WC can be seen that are distributed uniformly inside the MML (Fig. 14b). Underneath the MML, ultrafine grained and elongated grained Ni induced by plastic deformation was observed, where the modified layer was roughly 1-1.5 µm in thickness (Fig. 14c). Upon closer investigation inside the MML (Fig. 14d), a nanocrystalline structure was observed with a grain size of 4 - 10 nm. SAED was performed on the MML and resulting ring patterns, indicating the nano-crystalline structure was indexed. The d-spacing was compared with standard PDF card of NiO phase, which matched well to the d-spacing of the rings, indicating the presence of NiO in the nanocrystalline layer (Fig. 14d).

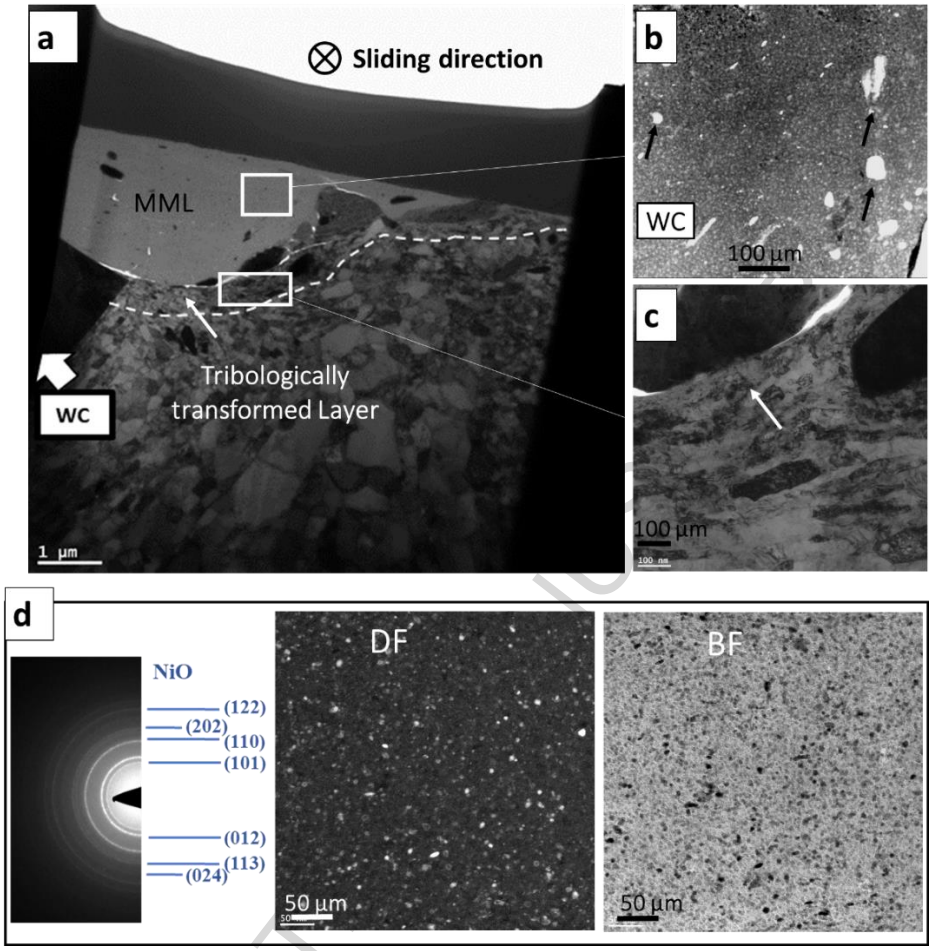

Fig. 14 (a) TEM images of Ni-castWC wear track surface cross-section (tested under 12 N), (b) upper inset shows high-angle annular dark-field (HAADF) image of WC distribution, (c) lower inset shows HAADF image of tribologically transformed layer at subsurface of wear track, (d) dark field and bright field of MML and SAED patterns of MML.

The MML thickness is relatively uniform across the worn surface for Ni-aggWC coating (Fig. 15a). WC fragments were distributed inside the MML, similar to the previous case (Fig. 15a). Underneath the MML, on the right side of the thin foil, a relatively large Ni particle was observed (Fig. 15b). This contained WC fragments and its microstructure was found to be similar to the

original microstructure of coating. However, on the left side of the thin foil, a sliding induced deformation zone, with ultrafine-grained (UFG) and elongated grains can be observed. Cracking can be observed nucleated and propagated inside the Ni particle, indicating large shear transferred to subsurface region. Similar to the Ni-castWC, the MML consisted of NiO as the major phase. However, EDX mapping and point analysis revealed some areas that were detected to be metallic Ni with significantly lower oxygen content compared to the surrounding areas (Fig. 15c and d).

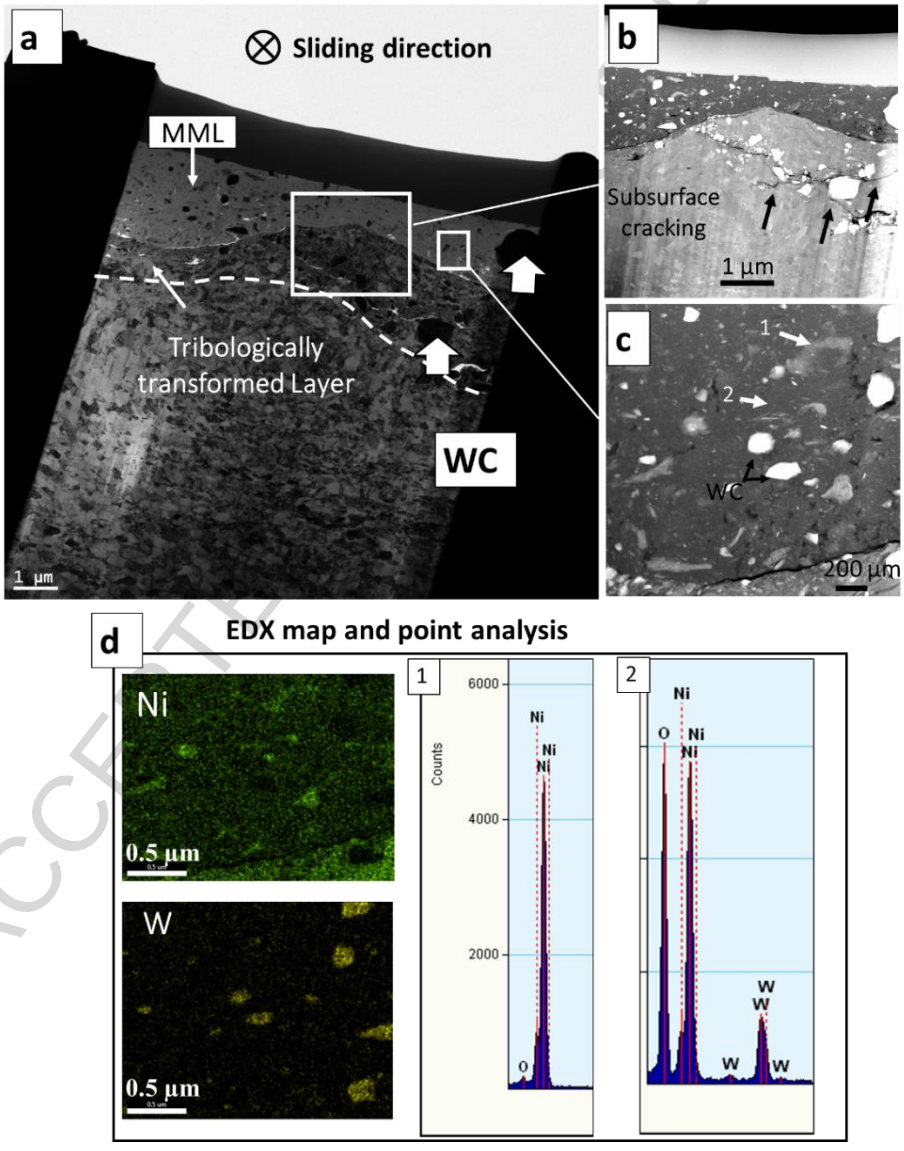

Fig. 15 (a) TEM images of Ni-aggWC wear track surface cross-section (tested under 12 N), (b) upper inset shows HAADF image of tribologically transformed layer at subsurface of wear track,

(c) lower inset shows the HAADF image of WC distribution at MML, (d) EDX map of the region (c) and EDX point analysis of points 1 and 2 in (c).

Nanoindentation was performed on worn surfaces (plan-view), where indentation tests were placed specifically onto MMLs to measure their hardness (Fig. 16 a and b). The load selected for the tests resulted in a depth of indentation on the order of 120 nm, which is much less than the typical 1.5 - 2 μm thickness of the MML. Nevertheless, there may be some 'substrate effect' from the underlying coating material, which was typically nanocrystalline Ni (e.g. Figures 14 and 15). Nanoindentation was also performed on cross-sections of worn surfaces, and nano-hardness profiles as a function of depth beneath the worn surface were obtained (Fig. 16a and b). The indentation profiles (e.g. Fig. 16 c and d) were carried out in regions beneath the MMLs, but the MMLs were typically not retained during the mounting and polishing of the cross-section. In Figure 16a and b, the MML hardness is significantly higher than that of the unworn coatings (see Table I). The hardness measured for the MMLs were similar. In fact, a t-test analysis showed that the difference between the MMLs mean nano-hardness values was not statistically significant with a confidence interval of 95%. For the subsurface hardness measurements from the cross-sections, the hardness values decreased and stabilized at some depths from the worn surface (Fig. 16). These match well with depths up to which the UFG layer (deformed zone) extended beneath the worn surfaces (Fig. 14a and 15a). For Ni-aggWC, tested under both loads, hardness values reached the unworn value at depth of around 6 μm from the worn surface. This was significantly lower (~3 μm) for Ni-castWC, indicating lower shear stresses transferred to the subsurface regions.

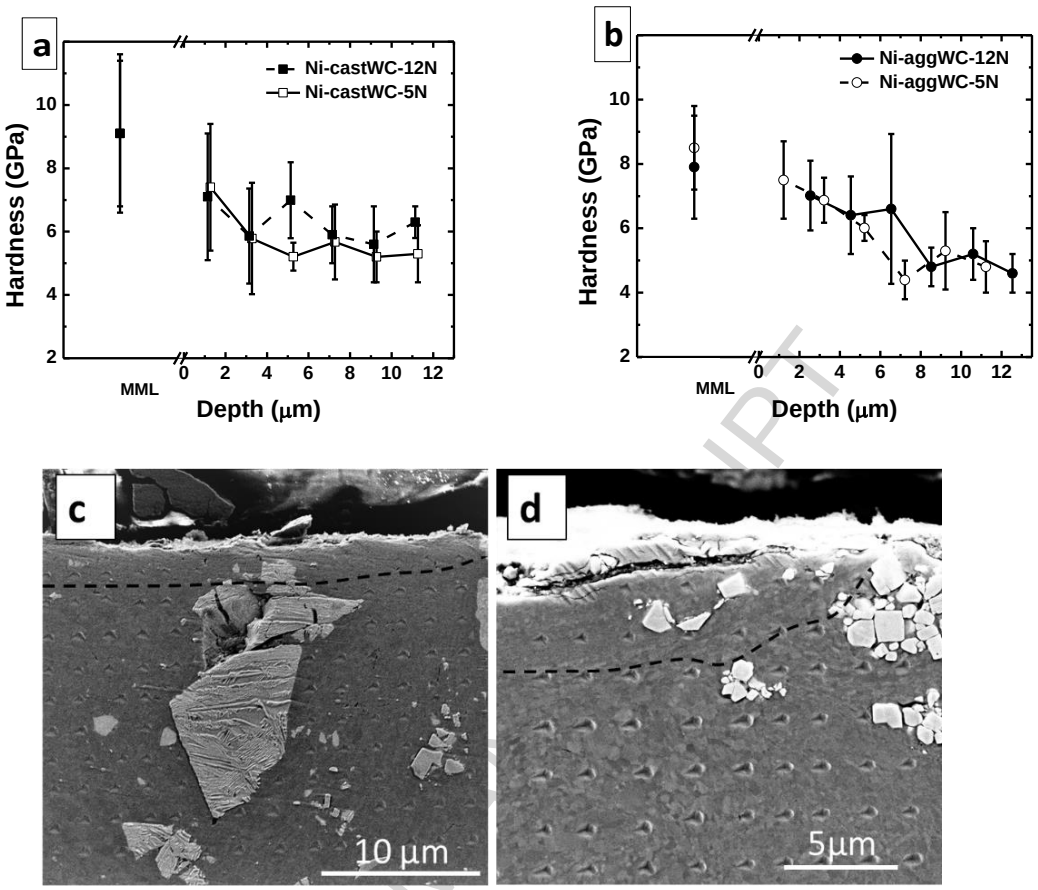

Fig. 16 Hardness of the MMLs and subsurface to worn surfaces of (a) Ni-castWC and (b) Ni-aggWC coatings tested at 5 and 12 N. (c) and (d) SEM micrograph containing part of the nanoindentation matrix of Ni-castWC and Ni-aggWC coatings, respectively, tested at 12 N. First data points in nano-hardness graphs (MML) indicates near surface MML hardness that are performed on worn surfaces plan-view. These measurements may have substrate effects. The data points on the hardness profile are cross-sectional indentation and are more confident. Trends on cross-sectional hardness profiles showed that deformation zones extended beneath MMLs to greater depth for Ni-aggWC as compared to Ni-castWC. Dashed lines indicate sliding induced deformation layer.

4. Discussion

Two Ni-WC coatings were cold sprayed using two different powder types, namely, cast WC and agglomerated WCNi, and then subjected to dry sliding wear testing. Due to the WC, the hardness of the coatings was increased as compared to cold sprayed Ni coatings (345 ± 17 HV_{1kg}) tested in a previous study [12]. The addition of hard particles also densified the coatings. Lower MFPs between WC particles (8.5 ± 0.7 µm versus 31 ± 4 µm in Ni-aggWC) and harder surface (431 ± 26 HV_{1kg} versus 390 ± 27 HV_{1kg} for Ni-aggWC) for Ni-castWC coatings was observed. The morphology of WC particles was found to influence the friction and wear behavior of the coatings under the two tested loads, 5 and 12 N. CoF analysis combined with microstructural and chemical examination demonstrated that friction and wear behavior were controlled by the behavior of third bodies and the supporting role of WC particles, both of which was modified by the morphology of WC particles.

For the Ni-aggWC, adhesion of Ni to the counterface initiated upon sliding (Fig. 7). Initial adhesion of coatings materials to countersphere led to pull-out of WC fragments (Fig. 7). This could be due to decohesion of WC fragments along weak interfaces of porosities or Ni binder. De-bonding and pull-out of WCNi particles from the Ni matrix is another possible case. Adhesive wear created large wear debris (Fig. 10) that were easier to eject from the interface and contributed to high initial wear rates in Ni-aggWC. This is supported by the observation of large debris at the ends of the wear tracks in initial cycles and high materials removal rates recorded. Some of the wear debris, generated at initial cycles at the contacting asperities, may leave the tribological system and some may remain trapped between the mating surfaces and damage on both surfaces [31]. The higher load led to higher initial wear rate.

Adhesive wear resistance of Ni-castWC was significantly enhanced due to the harder surface provided by cast WC particles and lower MFP between them. Much less adhesive wear was observed on the worn surfaces of the Ni-castWC tested under two loads. However, fine scratches were observed on both the center and sides of the wear tracks (Fig. 6). As the observation of WC fragments on the surface and size of the abrasive marks implied, only fine WC particles were dislodged from surfaces (Fig. 6). As reported by previous studies [20, 32], fine ceramic particles are more susceptible to being pulled out during the sliding process, whereas coarse particles are embedded deeply in the matrix and can be retained on the surface during wear test [20, 32]. Micro-ploughing in the direction of sliding along with light adhesion as the main wear initiation mechanism for Ni-castWC produced fine wear particles (Fig. 6).

As shown by Raman spectroscopy (Fig. 11a) and confirmed by the EDX analysis, for Ni-castWC coatings, oxidation of third-bodies started from early cycles. However, for Ni-aggWC longer cycles were needed for oxidation (Fig. 11b). The rate of the oxidation is controlled by debris size and the density of surface defects. Easy adhesion and flow of materials in the Ni-aggWC led to large wear particles with a lower oxidation rate, whereas due to the harder surface in Ni-castWC, plastic deformation was localized in the interfacial region. This created dislocations and voids, which increased the rate of tribo-oxidation by providing routes for passage of oxygen ions [33]. The oxidation was also accelerated in small debris with the higher relative surface area, which would increase the available surface energy [31, 33].

As sliding progressed, wear debris (metallic, oxide and carbides) were compacted between the sliding surfaces and developed progressively areas of wear-protective MMLs (Fig. 8 and 9). Formation of MMLs has been frequently reported during sliding wear testing of metallic and MMCs [18, 19]. Previous studies demonstrated that this not only reduced wear rate by recycling

of wear debris but also acted as a hard and protective layer for first bodies, since it consisted agglomeration of heavily deformed and oxidized wear debris [18, 19]. For the two coatings tested in this study, the formation of MML was found to reduce the wear rate and caused a drop in CoF, as well. However, the rate of MML formation, its coverage on the surfaces, as well as its effectiveness in reducing wear and stabilizing of friction for the two coatings are influenced by the morphology of the WC particles. There is a number of factors that favor the developing of MMLs and their stability. In Ni-aggWC, large wear particles were easily ejected from the interface. Those that stayed in contact behaved as in-situ elastic bodies and contributed to abrasive wear [34]. Whereas, for Ni-castWC, small debris that remained at interface, strain-hardened, fractured, and oxidized. The adhesion force existing between small particles led to agglomeration and formation of protective MMLs to a higher coverage [19].

For both coatings studied here, the small WC fragments of nano- to sub-micron size, were observed to be embedded into MMLs (Fig. 8 and 9). These particles can be carried away when the MML becomes unstable. In the Ni-aggWC coating, WC fragments are 0.3 - 1.3 μm size, smaller than critical oxide thickness (1-5 μm). Whereas, a multimodal distribution with a size ranges of 0.2 to 20 μm was established for Ni-castWC during cold spray deposition (Fig. 9). Smaller particles are moved away when the oxide layer is broken, whereas large WC particles stand exposed in the interface and reinforced metals from severe wear damage (see Fig. 17). No pull-out of coarse WC particles was observed, even though they are only mechanically bonded to the matrix. Examination of cross-sections of the wear surfaces also revealed that the MML thickness was higher (~2.4 μm) when it is supported by coarse WC particles (Fig. 14a). This may imply that the supporting effect of hard coarse particles to oxide film makes it stable at the higher thickness, i.e. increasing "oxide critical thickness". MMLs formed on Ni-castWC coatings were found to be more effective in reducing wear when compared to that formed on Ni-aggWC coatings (see Fig. 17).

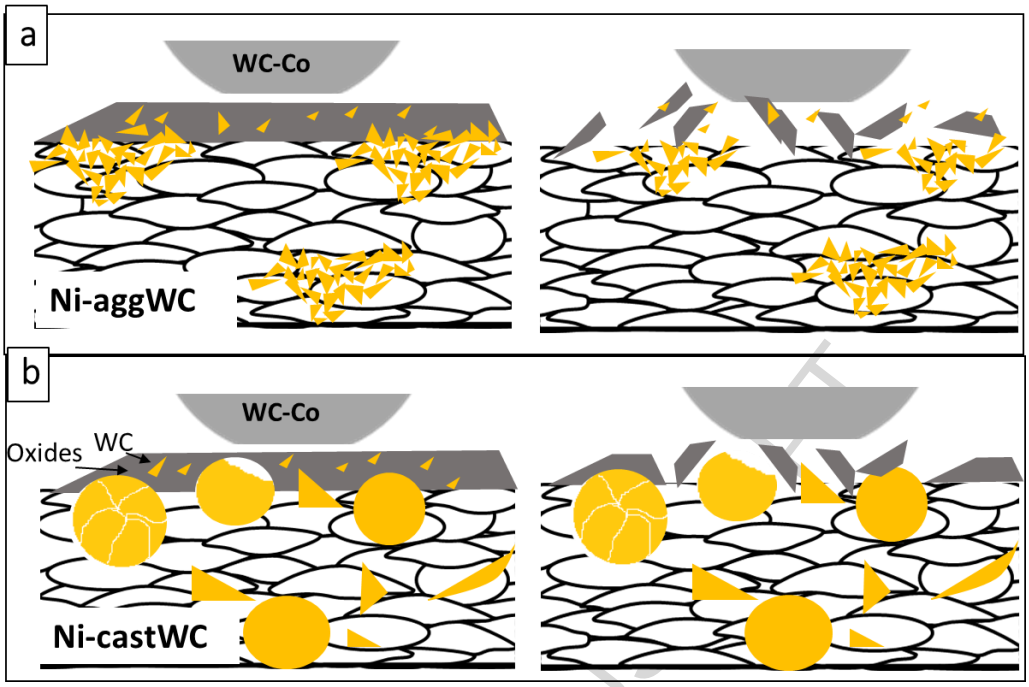

Fig. 17 A schematic diagram showing MML development in the presence of agglomerated WCNi in (a) Ni-aggWC and cast WC in (b) Ni-castWC; WC fragments are drawn by the oxide when it breaks up to form wear debris in Ni-aggWC; large WC particles remain in place when the oxide breaks up in Ni-castWC.

For both coatings, as revealed by electron diffraction of the cross-section of wear surfaces, NiO is dominating phase in the MML. Since it is less Raman active than Co/NiWO4 and WO_3 a weaker peak was obtained in the Raman spectra. Chemical analysis of the MMLs on the worn surfaces, performed by Raman spectroscopy, showed for both coatings formation of tribochemical phases of WO_3 and Co/$NiWO_4$ (Fig. 11). Previous studies [30, 35-37] reported the formation of these phases during room and elevated temperature sliding of Ni-WC coatings. It is proposed that Co/$NiWO_4$ form due to the interfacial mixing of Co/NiO and WO_3 during sliding. Raman analysis revealed that the MML of Ni-castWC contained a higher amount of Co/$NiWO_4$, whereas the MML of Ni-aggWC mainly consisted of NiO and WO_3. While for Ni-aggWC, some regions inside the MML with significantly low oxygen content were detected in the cross-section of wear tracks.

This, along with large flakelike particles observed on the wear track (Fig. 10) and counter-body (Fig. 12), also implied that the particles did not get sufficiently oxidized before they are dislodged from the sliding surfaces. Moreover, cracking was observed due to large shear stress transferred to subsurface regions, which imply the low load-bearing capacity of both MMLs and subsurface. The intersection of these cracks led to detachment of wear particles by delamination process. The hard particles detached from MML, which were frequently observed in Ni-aggWC tested under 5 N, acted as third-bodies abrasive particles, which induced wear on sliding surfaces and resulted in increased wear rate and unstable CoF. A higher wear rate was recorded for Ni-aggWC at 12 N. Although some cracks were observed on the MMLs surfaces and cross-sectional view of Ni-aggWC at 12 N, however, smooth MMLs and significantly lower amounts of wear debris along with a high initial wear rate inferred that most of the wear occurred during initial sliding cycles. At subsequent sliding cycles, the higher frictional heat generated under high load resulted in a temperature rise in the contacting regions, and hence, sintering the debris. Increasing normal load can promote mechanical mixing effects on entrapped particles, and then boost the oxidation process, as well.

WC containing MMCs generally are expected to have greater than 50% WC (often > 70%) to be a wear-resistant, hard-facing coating [1]. For cold spray, it is difficult to retain such high-volume fractions of WC, as the main deposition mechanism is adiabatic shear of the metal particles [7]. WC particles interrupt this process and the more WC in the feedstock, the more ceramic-ceramic collisions occur, that also lead to a reduction of deposition and retention of WC. In our recent study [13], the highest retention for cast WC was and agglomerated WC was 28 and 54 vol.%, respectively. Moreover, the agglomerated powder had higher deposition efficiencies [13]. Based on this, the temptation is the use of agglomerated powder to retain more WC. However, for the highest retention in Ni-aggWC coatings, the coating was thin and cracked [13]. Also, as was

demonstrated here for a side-by-side comparison of coatings made from the two WC powder types, the cast-WC leads to better tribological properties. This is because of the formation of more stable MMLs that lead to better wear resistance. The subsurface microstructure plays a role in wear resistance. In both coating systems, MMLs eventually cracked and detached, but this was more extensive in the Ni-aggWC coating. This was due to the lack of load support from the underlying coating. This was discussed with respect to Fig. 14 and 15, where large particles in the cast WC coating provided load support, while having only small-sized WC in the Ni-aggWC coating did not provide any load support. Thus, as the slider passes over the MML, there is greater strain induced in the MML on the Ni-aggWC coating compared to the Ni-castWC coatings. This leads to faster cracking and breaking of the MMLs on the Ni-aggWC coating. One can also envision that after MML breakage, that the near surface hard WC particles in the cast coating are more efficient at "re-mixing" the detached MML and creating new adherent MMLs.

Other researchers studying WC containing coating by cold spray have shown microstructures with higher WC content [9-11], but have not demonstrated clearly whether these coatings are wear resistant. Here we have shown that powder selection is critical and high retention does not necessarily produce the best wear resistance. Also, engineering a powder for high ceramic retention does not necessarily impart the best tribological properties as was seen for the agglomerated WCNi powder. Other factors play a role, such as cohesion of particles within the coating, MFP between WC particles and their size distribution within the coating. As a result, the cold spray process is not yet able to produce a very high fill ratio WC containing MMC with optimal tribological properties. More powder engineering and process optimization will need to be carried out to make this possible. However, with the present study, we have shown wear mechanisms and important factors for coating microstructure to impart the best wear resistant properties. It may also be the case that cold sprayed WC based MMCs with a lower fill ratio of WC

will have acceptable properties for some applications and as a repair option for higher performing coatings with high fill ratio.

5. Conclusion

A side-by-side comparison of tribological performance was conducted on two Ni-WC composite coatings prepared by cold spray using cast and agglomerated WC powders. The two coatings had nearly identical WC content, but very different size distribution and MFP between WC particles. These features led to distinctly different wear mechanisms and tribological performance. In early cycles, the lower MFP in the Ni-castWC coating made this coating more resistant to adhesive wear compared to the Ni-aggWC coating. As wear progressed, the wear mechanism shifted to primarily tribo-oxidative wear. Again, the nature of the WC in the Ni-castWC was more effective at resisting wear. The larger-sized WC in these coatings were load supporting, resulting in less cracking and removal of the MMLs formed by tribo-oxidation. In the Ni-aggWC coatings, WC particles were very small and offered very little load-support by comparison and as a result, more significant cracking and removal of MMLs was observed. For both coatings, the MML was primarily nano-crystalline NiO, with some metallic Ni and WC also present. Raman spectroscopy also showed the presence of WO_3 and $NiWO_4$, which were likely present in very small quantities at the worn surfaces. Overall, the Ni-castWC was wear resistant under both loads tested (5 and 12 N). For the Ni-aggWC, it was similarly wear resistant at 5 N, but had a five-fold increase in wear rate when tested at 12 N. The poorer wear resistance for the Ni-aggWC coating was linked to the inability to resist adhesive wear in early stages of wear and then lack of load-support for the MMLs in later stages of wear.

It is important to note that, for conditions tested here, wear resistance for the cold sprayed composites was not simply linked to the presence of third bodies (i.e. the MMLs) and their properties. Instead, the wear resistance was related to the stability of the MMLs, which was

dependent significantly on the starting microstructure. With this knowledge, agglomerated powders, which are engineered for higher WC retention in cold spray, were found to not always impart the best tribological properties compared to other options (e.g. cast WC powders). Size, morphology, and distribution of the WC particles in the coatings had a significant impact on the stability of MMLs, the third body flows, and wear resistance. Future research on cold sprayed metal matrix composites containing WC or other hard phases should consider these factors when designing or selecting powders and spray conditions.

Acknowledgments

The authors gratefully acknowledge the financial support from the Canadian Foundation for Innovation (CFI) project No. 8246 for the cold spray equipment, the CFI Leader's Opportunity Fund project No. 13029 for the tribometer and nanoindentation equipment, and the Natural Sciences and Engineering Research Council (NSERC) Strategic Grants Program for the operational funding of this project. Thanks, are also due to Tekna Inc for providing the Ni and spherical WC powders. The authors acknowledge administrative support from Drs. Phuong Vo, Eric Irissou and Jean-Gabriel Legoux and technical support from Mr. Jean Francois Alarie at the McGill Aerospace Materials and Alloy Design Center (MAMADC) cold spray facility at NRC-Boucherville.

References

[1] J.R. Davis, Introduction to Thermal Spray, ASM International and the Thermal Spray Society2004.
[2] Y.P. Kathuria, Some aspects of laser surface cladding in the turbine industry, Surf Coat Tech, 132 (2000) 262-269.
[3] M.R. Fernandez, A. Garcia, J.M. Cuetos, R. Gonzalez, A. Noriega, M. Cadenas, Effect of actual WC content on the reciprocating wear of a laser cladding NiCrBSi alloy reinforced with WC, Wear, 324 (2015) 80-89.
[4] K. Van Acker, D. Vanhoyweghen, R. Persoons, J. Vangrunderbeek, Influence of tungsten carbide particle size and distribution on the wear resistance of laser clad WC/Ni coatings, Wear, 258 (2005) 194-202.
[5] W. Su, Y. Sun, J. Feng, J. Liu, J. Ruan, Influences of the preparation methods of WC–Co powders on the sintering and microstructure of coarse-grained WC–8Co hardmetals, International Journal of Refractory Metals and Hard Materials, 48 (2015) 369-375.
[6] F.G. X.L. Jiang, M. Boulos, R. Tiwari, , Reactive deposition of tungsten and titanium carbides by induction plasma, J Mater Sci Lett, 30 (1995) 2325-2329.
[7] A. Papyrin, Cold Spray Technology, illustrated ed., Amsterdam ; London : Elsevier2007.
[8] V.K. Champagne, The cold spray materials deposition process : fundamentals and applications, Cambridge : Woodhead ; Boca Raton : CRC Press2007.
[9] D. Lioma, N. Sacks, I. Botef, Cold gas dynamic spraying of WC-Ni cemented carbide coatings, Int J Refract Met H, 49 (2015) 365-373.
[10] S. Yin, E.J. Ekoi, T.L. Lupton, D.P. Dowling, R. Lupoi, Cold spraying of WC-Co-Ni coatings using porous WC-17Co powders: Formation mechanism, microstructure characterization, and tribological performance, Materials & Design, 126 (2017) 305-313.
[11] N.M. Melendez, A.G. McDonald, Development of WC-based metal matrix composite coatings using low-pressure cold gas dynamic spraying, Surf Coat Tech, 214 (2013) 101-109.
[12] S.A. Alidokht, P. Manimunda, P. Vo, S. Yue, R.R. Chromik, Cold spray deposition of a Ni-WC composite coating and its dry sliding wear behavior, Surf Coat Tech, 308 (2016) 424-434.
[13] S.A. Alidokht, P. Vo, S. Yue, R.R. Chromik, Cold Spray Deposition of Ni and WC-Reinforced Ni Matrix Composite Coatings, J Therm Spray Techn, 26 (2017) 1908-1921.
[14] H.L.d.V. Lovelock, Powder/processing/structure relationships in WC-Co thermal spray coatings: A review of the published literature, J Therm Spray Techn, 7 (1998) 357–373.
[15] C.P. Bergmann, J. Vicenzi, Protection against Erosive Wear Using Thermal Sprayed Cermet: A Review, Springer Berlin Heidelberg,2011.
[16] B. Venkataraman, G. Sundararajan, Correlation between the characteristics of the mechanically mixed layer and wear behavior of aluminum, Al-7075 alloy and Al-MMCs, Wear, 245 (2000) 22-38.
[17] J.M. Shockley, H.W. Strauss, R.R. Chromik, N. Brodusch, R. Gauvin, E. Irissou, J.G. Legoux, In situ tribometry of cold-sprayed Al-Al2O3 composite coatings, Surf Coat Tech, 215 (2013) 350-356.
[18] J.R. Jiang, F.H. Stott, M.M. Stack, The role of triboparticulates in dry sliding wear, Tribology International, 31 (1998) 245-256.
[19] J.R. Jiang, F.H. Stott, M.M. Stack, Some Frictional Features Associated with the Sliding Wear of the Nickel-Base Alloy N80a at Temperatures to 250C, Wear, 176 (1994) 185-194.
[20] C.C. Degnan, P.H. Shipway, J.V. Wood, Elevated temperature sliding wear behavior of TiC-reinforced steel matrix composites, Wear, 251 (2001) 1444-1451.

[21] M. Vardavoulias, The role of hard second phases in the mild oxidational wear mechanism of high-speed steel-based materials, Wear, 173 (1994) 105-114.
[22] T.F.J. Quinn, Oxidational Wear, Wear, 18 (1971) 413-419.
[23] N.M. Melendez, V.V. Narulkar, G.A. Fisher, A.G. McDonald, Effect of reinforcing particles on the wear rate of low-pressure cold-sprayed WC-based MMC coatings, Wear, 306 (2013) 185-195.
[24] M. Kouzeli, A. Mortensen, Size dependent strengthening in particle reinforced aluminium, Acta Materialia, 50 (2002) 39-51.
[25] P. Chivavibul, M. Watanabe, S. Kuroda, J. Kawakita, M. Komatsu, K. Sato, J. Kitamura, Effect of powder characteristics on properties of warm-sprayed WC-Co coatings, J Therm Spray Techn, 19 (2010) 81-88.
[26] W.C. Oliver, G.M. Pharr, An Improved Technique for Determining Hardness and Elastic-Modulus Using Load and Displacement Sensing Indentation Experiments, J Mater Res, 7 (1992) 1564-1583.
[27] B. Bhushan, Principles and Applications of Tribology, Second ed., John Wiley & Sons2013.
[28] J.M. Guilemany, S. Dosta, J.R. Miguel, The enhancement of the properties of WC-Co HVOF coatings through the use of nanostructured and microstructured feedstock powders, Surface and Coatings Technology, 201 (2006) 1180-1190.
[29] K.L. Johnson, Contact Mechanics, Cambridge University Press, Cambridge, 1985.
[30] G. Bolelli, L.M. Berger, M. Bonetti, L. Lusvarghi, Comparative study of the dry sliding wear behaviour of HVOF-sprayed WC-(W,Cr)(2)C-Ni and WC-CoCr hardmetal coatings, Wear, 309 (2014) 96-111.
[31] G. Straffelini, Wear Mechanism, In: Friction and Wear Methodologies for Design and Control, Springer International Publishing, Switzerland, 2015.
[32] S. Mahdavi, F. Akhlaghi, Effect of the SiC particle size on the dry sliding wear behavior of SiC and SiC–Gr-reinforced Al6061 composites, J Mater Sci, 46 (2011) 7883.
[33] I.A. Inman, S. Datta, H.L. Du, J.S. Burnell-Gray, Q. Luo, Microscopy of glazed layers formed during high temperature sliding wear at 750 degrees C, Wear, 254 (2003) 461-467.
[34] H. Heshmat, The Rheology and Hydrodynamics of Dry Powder Lubrication, Tribol T, 34 (1991) 433-439.
[35] M.W. L.M. Berger, S. Saaro, Comparison of self-mated hardmetal coatings under dry sliding conditions up to 600◦C, Wear 266 (2009) 406–416.
[36] S.S. L.M. Berger, T. Naumann, M.Kasparova, F. Zahalka, Microstructure and Properties of HVOF-Sprayed WC-(W,Cr)2C-Ni Coatings, J Therm Spray Techn, 17(3) (2008) 395–403.
[37] A.W. Z. Weng, X. Wu, Y. Wang, Z. Yang, Wear resistance of diode laser-clad Ni/WC composite coatings at different temperatures, Surf Coat Tech, 304 (2016) 283-292.

Table I Characteristics of cold-sprayed Ni-castWC and Ni-aggWC coatings.

Figures Captions

Fig. 1 Secondary electron (SE) images of unworn microstructures of (a) Ni-castWC and (b)Ni-aggWC viewed in the cross-section.

Fig. 2 Representative coefficient of friction versus sliding distance at 5 and 12 N of cold sprayed Ni-castWC and Ni-aggWC coatings.

Fig. 3 Wear track topography of Ni-castWC at 5 N(a) and 12 N(b), and Ni-aggWC at 5 N(c) and 12 N(d).

Fig. 4 Volumetric wear rate for Ni-castWC and Ni-aggWC tested at (a) 5 N and (b)12 N.

Fig. 5 Volumetric wear rate at 1000 cycles plotted for counter-spheres mating with Ni-castWC and Ni-aggWC coatings at 5 and 12 N.

Fig. 6 Wear track topography of Ni-castWC after 10cycles (a) and (c), 50 cycles (b) and (d) at 5 and 12 N, respectively. Black arrows show scratching marks.

Fig. 7 Wear track topography of Ni-aggWC after 10cycles (a) and (c), 50 cycles (b) and (d) at 5 and 12 N, respectively. Black arrows show adhesive wear. White arrows indicate WC dislodgments.

Fig. 8 Wear track topography of Ni-castWC after 1000cycles (a) at 5 N, (c) at 12 N, (b) and (d) higher magnification BSE images of (a) and (c), respectively.

Fig. 9 Wear track topography of Ni-aggWC after 1000cycles (a) at 5 N, (c) at 12 N, (b) and (d) high magnification BSE images of (a) and (c), respectively. Black arrows show wear debris. Inset in (a) and (c) shows cracking and plate-like debris formation.

Fig. 10 Morphology of wear debris outside the wear track of (a) and (b) Ni-castWC, (c) and (d) Ni-aggWC tested under 5 and 12 N, respectively.

Fig. 11 Raman spectra of the MMLs obtained from (a) Ni-castWC and (b) Ni-aggWC coatings, (c) a typical EDX spectra obtained from MML of composite coatings.

Fig. 12 SEM images of WC-Co counterfaces after 1000 cycles sliding on (a) Ni-castWC coating and (b) Ni-aggWC, under 12 N, (c) Raman spectra of wear debris on the WC-Co counterfaces. The arrows in the SEM images indicate the location for each Raman spectra.

Fig. 13 Location of TEM foils obtained through FIB cutting on wear track of (a) Ni-castWC and (b) Ni-aggWC after 1000 cycles of wear under 12 N.

Fig. 14 (a) TEM images of Ni-castWC wear track surface cross-section (tested under 12 N), (b) upper inset shows high-angle annular dark-field (HAADF) image of WC distribution, (c) lower inset shows HAADF image of tribologically transformed layer at subsurface of wear track, (d) dark field and bright field of MML and SAED patterns of MML.

Fig. 15 (a) TEM images of Ni-aggWC wear track surface cross-section (tested under 12 N), (b) upper inset shows HAADF image of tribologically transformed layer at subsurface of wear track, (c) lower inset shows HAADF image of WC distribution at MML, (d) EDX map of the region (c) and EDX point analysis of points 1 and 2 in (c).

Fig. 16 Hardness of the MMLs and subsurface to worn surfaces of (a) Ni-castWC and (b) Ni-aggWC coatings tested at 5 and 12 N. (c) and (d) SEM micrograph containing part of the nanoindentation matrix of Ni-castWC and Ni-aggWC coatings, respectively, tested at 12 N. First data points in nano-hardness graphs (MML) indicates near surface MML hardness that are performed on worn surfaces plan-view. These measurements may have substrate effects. The data points on hardness profile are cross-sectional indentation and are more confident. Trends on cross-sectional hardness profiles showed that deformation zones extended beneath MMLs to greater depth for Ni-aggWC as compared to Ni-castWC. Dashed lines indicate sliding induced deformation layer.

Fig. 17 A schematic diagram showing MML development in the presence of agglomerated WCNi in (a) Ni-aggWC and cast WC in (b) Ni-castWC; WC fragments are drawn by the oxide when it breaks up to form wear debris in Ni-aggWC; large WC particles remain in place when the oxide breaks up in Ni-castWC.

Highlights:

- Two types of WC particles, i.e. cast and agglomerated, were cold-sprayed with Ni.
- Cast WC led to a lower mean free path between WC particles than agglomerated.
- Cast WC was more effective in improving wear resistance of composite coatings.
- Cast WC minimized adhesive wear at initial cycles of wear.
- Cast WC aided to develop a higher coverage of protective mechanically mixed layer.